Jour. of the KGS, Vol. 20, No. 7. September 2004, pp. 207~215

Analysis on the Geo-reinforced Slope Using Upper Bound Theory

상계해석을 이용한 보강토 사면의 해석

Choi, Sang-Ho[1] 최 상 호
Kim, Jong-Min[2] 김 종 민
Yu, Nam-Jae[3] 유 남 재

요 지

본 연구는 보강사면에 상계이론를 적용하여 실제 한계상태에 가까운 신뢰성이 높은 해석방법을 개발하는데 목적이 있으며 상계해석의 유한요소공식화를 전개하는데 있어 거시적인 관점으로부터 비등방성이면서 균질한 재료에 대한 수치해석의 기본 개념은 얻을 수 있다. 보강토는 뒷채움한 성토와 보강재 경계면의 상호작용으로 보강토의 강도가 보강재의 재료적 특성에 의존하고 있기 때문에 흙의 역학적 특성과 보강토의 전체 거동은 보강재의 기하학적인 배열과 상대적인 면적에 의해서 조절할 수 있다. 따라서, 상계이론은 보강사면의 한계상태 거동을 효과적으로 산정할 수 있어 국부적으로 발생하는 소성파괴를 예측할 수 있다.

Abstract

In this study, the upper bound theory is applied to a reinforced slope to develop an limit state analysis method. As processing of this upper bound theory in formulating finite element, the basic idea of numerical method can be obtained from a macroscopic point of view with an anisotropic homogeneous material. The reinforced soil strength reliability depends on properties of reinforcements which consist of the interaction of interfaces between back fill and reinforcements. Both soil's mechanical property and overall behaviour of reinforced soil can be controlled via arranging geometry and relative proportions of reinforced soil. Therefore, the upper bound theory can not only predict the particular limit state action of reinforced soil slope but also is efficiently able to estimate the local plastic failure.

Keywords : Homogenisation, Limit analysis, Reinforced slope, Slope stability, Upper bound analysis

1. Introduction

Due to the economical efficiency and conveniency, the reinforced soil structure has been increasingly constructed around the world. Although the stability analysis method of reinforced soil has been studied for decades by many researchers, most studies were based on limit equilibreum method which is known to be lacking in mechanical rigor. The analysis of reinforced soil structure requires reliable analysis method that will demonstrate the limit state of structure.

The upper bound theory based on plastic limit theorem and perfectly rigid plastic model is able to assess the stability of variable soil structures by predicting collapse load causing plastic failure.

In this study, upper bound analysis method for reinforced slope is developed using homogenisation technique so that reinforced soil slope can be treated like

1 Member, Graduate Student, Dept. of Civil, Univ. of Sejong (civilgeo@sju.ac.kr)
2 Member, Assistant Prof., Dept. of Civil, Univ. of Sejong
3 Member, Graduate Student, Dept. of Civil, Univ. of Sejong

homogeneous and anisotropic material.

Parameters required for analysis can be obtained from material strengths characteristics. The homogenisation approach to a limit analysis procedures of reinforced soil has proven to be efficient from recent studies of reinforced foundations and retaining walls.

In the development of numerical analysis methods to attain the exact or upper bound solution of reinforced soil slope, finite element method is used for modeling and Mohr-Coulomb failure criterion is properly modified for homogenisation of reinforcement and soil.

Mohr-Coulomb failure criterion is modified to consider the influences of both reinforced soil's shear stress on interface and vertical stress of overall reinforced slope, so that the upper bound theory can be formulated with homogenisation condition for numerical analysis.

The upper bound theory is able to acquire the better results of true failure loads with proper boundary conditions. Using the boundary condition of finite element formulation for reinforced slope, the upper bound theory can estimate the stability of slope conveniently.

2. Failure Condition For Reinforced Soils

In actual state, the reinforced slope consists of inhomogeneous and anisotropic material. In order to treat reinforced slope as a continuum mass, homogenisation technique is used as shown in Fig. 1.

This assumption which can be described by three stress tensors in all nodes is able to substitute the soil's macrostress and microstress, σ^s, σ^r, respectively.

In Fig. 1, the thickness of reinforcements is characterized as d and the vertical space between reinforcements is h. The thickness of reinforcements, d is comparatively smaller than vertical space, therefore this stress state can be written as Eq. (1)

$$\sigma_x^s = \sigma_x - \sigma^r, \qquad \sigma_y^s = \sigma_y, \qquad \tau_{xy}^s = \tau_{xy} \tag{1}$$

where, σ^r is the axial tensile stress acting in the reinforcement times $\frac{d}{h}$.

It is possible to express relationship between the vertical stress and shear stress using macrostress and microstress as follows.

$$\sigma_n = \sin^2\theta\sigma_x + \cos^2\theta\sigma_y - \sin 2\theta\tau_{xy},$$
$$\tau = -\frac{1}{2}\sin 2\theta\sigma_x + \frac{1}{2}\sin 2\theta\sigma_y + \cos 2\theta\tau_{xy} \tag{2}$$

The difference between σ and σ^s was resolved on x-y plane and then it is assumed that the reinforcement in soil mass does not resist against any shear strengths, moments, nor compressions. σ^r has a constant value of $0 \le \sigma^r \le \sigma_0$ and σ_0 can also be expressed as $\frac{d}{h}\sigma_{yield}$, in terms of actual tensile yield strength, reinforcements and

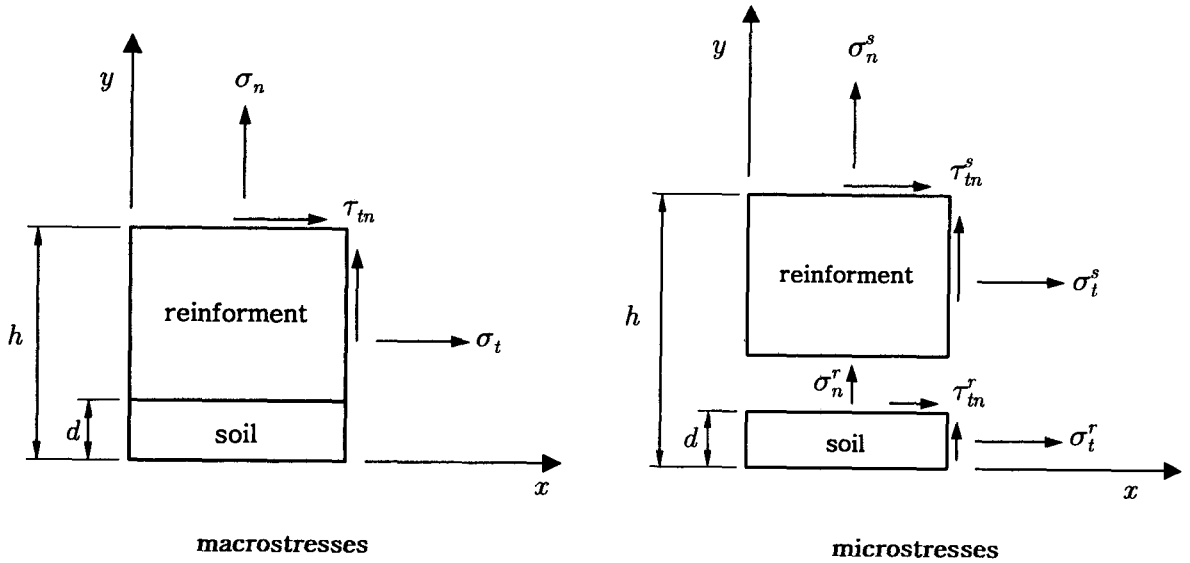

Fig. 1. Stresses on reinforcement

thickness of reinforcements. Soil mass following Mohr-Coulomb criterion has a positive value of tensile stress in plane strain condition.

$$F_s = (\sigma_x^s - \sigma_y^s)^2 + (2\tau_{xy}^s)^2 - (2c\cos\phi - (\sigma_x^s + \sigma_y^s)\sin\phi)^2 = 0 \quad (3)$$

Considering the influences of the effectiveness of reinforcements, Mohr-Coulomb criterion can be written in terms of macrostress and tensor as follows

$$F_s = (\sigma_x - \sigma_y - \sigma^r)^2 + (2\tau_{xy})^2 - (2c\cos\phi - (\sigma_x + \sigma_y - \sigma^r)\sin\phi)^2 = 0 \quad (4)$$

Buhan & Siad (1989) proposed the influence of interface between soil and reinforcement, based on failure criterion of reinforcement and macro behaviour of soil by selecting cohesion and internal friction angle of interface.

From Buhan & Siad's study, the limit strength of interface is represented as functions of cohesion and internal friction angle in Eq. (5).

$$F_i = |\tau| - c_i + \sigma_n \tan\phi_i = 0 \quad (5)$$

where, τ = shear stress; σ_n = normal stress; and c_i, ϕ_i = interface cohesion and interface friction angle respectively.

In addition it is possible to rewrite the yield criterion of interface in terms of a macrostress tensor in adopting the stress transformation relations as follows.

$$F_i = \tau_{xy} - c_i + \sigma_y \tan\phi_i = 0 \quad (6)$$

3. Upper Bound Theorem

3.1 Introduction

The upper bound theory has been applied to the stability analysis of various geotechnical structures. Since there are a number of kinematically admissible velocity fields for a given soil mass, analytical method is hard to get the true failure condition for the upper bound analysis. on the other hand, introduction of numerical analysis can solve the problems which can not solved by analytical method. In upper bound theory, by modeling a given soil mass using finite element, kinematically admissible velocity field can be defined as functions of nodal and elemental variables of finite elements.

By applying optimization technique, the most critical failure state of kinematically admissible velocity field can be obtained. In this study, nodal and elemental variables are used for objective function and constraint equations of optimization programming.

3.2 The Characteristic of Finite Element and Finite Element Meshes

In this study, to make optimization problem as a linear programming, the nodal velocities, undefined vertical and horizontal velocity, of finite element for the upper bound analysis are used for linearizing yield condition.

For upper bound analysis, triangular finite element with linear shape function is used as shown in Fig. 2. Therefore, a node of finite element mesh will have more than two identical coordinates. The linear variation of nodal velocity is calculated by Eq. (7).

$$u = \sum_{i=1}^{3} N_i u_i, \quad v = \sum_{i=1}^{3} N_i v_i \quad (7)$$

where, N_i = linear shape function; u_i, v_i = nodal variables as node i.

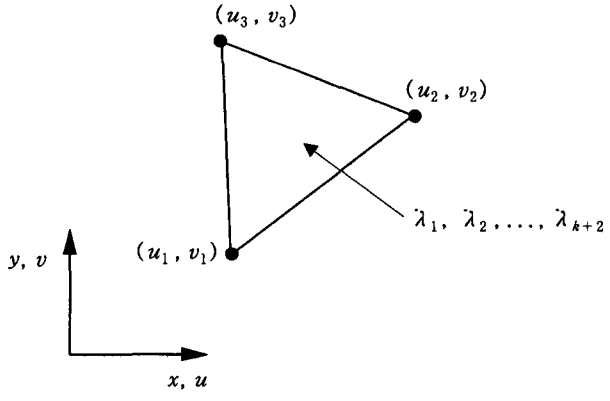

Fig. 2. Three noded velocity element for upper bound analysis

3.3 Formulations of Requirement for Kinematically Admissible Velocity Field

3.3.1 Plastic Flow within an Element

In order to construct a kinematically admissible velocity fields, the related flow rule must be satisfied as expressed by Eq. (8).

$$\dot{\varepsilon}_x = \frac{\partial u}{\partial x} = \dot{\lambda}\frac{\partial F}{\partial \sigma_x}, \quad \dot{\varepsilon}_y = \frac{\partial v}{\partial y} = \dot{\lambda}\frac{\partial F}{\partial \sigma_y},$$
$$\dot{\gamma}_{xy} = \frac{\partial v}{\partial x} + \frac{\partial u}{\partial y} = \dot{\lambda}\frac{\partial F}{\partial \tau_{xy}} \tag{8}$$

where, $\dot{\varepsilon}_x$, $\dot{\varepsilon}_y$, $\dot{\gamma}_{xy}$= plastic strain rate; $\dot{\lambda}$= non-negative plastic multiplier rate; F= yield function.

Along with conditions by Eq (8), the kinematically admissible velocity field is defined by equations of the boundary condition of velocity discontinuities and related flow rules. After eliminating the stress terms in those equations by the integration, the yield criterion can be expressed as a linear function. Under plane strain condition, Mohr-Coulomb yield criterion can be approximated by a linear polygon circumscribing a circle as shown in Fig. 3.

If yield criterion is linearized by p-polygon, it can be expressed by Eq. (9).

$$F_k = A_k\sigma_x + B_k\sigma_y + C_k\tau_{xy} - D_k = 0 \quad \text{for}$$
$$k = 1, 2, \ldots, p+2 \tag{9}$$

where, $A_k = \cos(\frac{2\pi k}{p}) + \sin\phi$;

$B_k = -\cos(\frac{2\pi k}{p}) + \sin\phi$; $C_k = 2\sin(\frac{2\pi k}{p})$;

$D_k = 2c\cos\phi + \sigma_0[\sin\phi + \cos(2\theta - \frac{2\pi k}{p})]$.

The yield function between soil and geo-reinforcements is the same as Eq. (9), which considers the influence of reinforcement. In order to consider the influence of cohesion on interface, Eq. (10) must be added to Eq. (9).

$$D_{p+1} = D_{p+2} = c_i \quad \text{for} \quad k = p+1,\ p+2 \tag{10}$$

For this linearised yield function, considering the effect of soil reinforcement and soil-reinforcement interface, an associated flow rule is appled for the calculation of plastic strain rates throughout each triangular elements as in Eq. (11).

$$\dot{\varepsilon}_x = \frac{\partial u}{\partial x} = \dot{\lambda}\frac{\partial F}{\partial \sigma_x} = \sum_{k=1}^{p+2}\dot{\lambda}\frac{\partial F_k}{\partial \sigma_x} = \sum_{k=1}^{p+2}\dot{\lambda}_k A_k$$
$$\dot{\varepsilon}_x = \frac{\partial v}{\partial y} = \dot{\lambda}\frac{\partial F}{\partial \sigma_y} = \sum_{k=1}^{p+2}\dot{\lambda}\frac{\partial F_k}{\partial \sigma_y} = \sum_{k=1}^{p+2}\dot{\lambda}_k B_k$$
$$\dot{\gamma}_{xy} = \frac{\partial v}{\partial x} + \frac{\partial u}{\partial y} = \dot{\lambda}\frac{\partial F}{\partial \tau_{xy}} = \sum_{k=1}^{p+2}\dot{\lambda}\frac{\partial F_k}{\partial \tau_{xy}} = \sum_{k=1}^{p+2}\dot{\lambda}_k C_k \tag{11}$$

In numerical analysis, Eq. (11) can be expressed as Eq. (12).

$$[A_{11}^e][x_1] - [A_{12}^e][x_2] = 0 \tag{12}$$

where, A_{11}^e = differential term of shape function

$$= \frac{1}{2A}\begin{bmatrix} y_{23} & 0 & y_{31} & 0 & y_{12} & 0 \\ 0 & x_{32} & 0 & x_{13} & 0 & x_{21} \\ x_{32} & y_{23} & x_{13} & y_{31} & x_{21} & y_{12} \end{bmatrix};$$

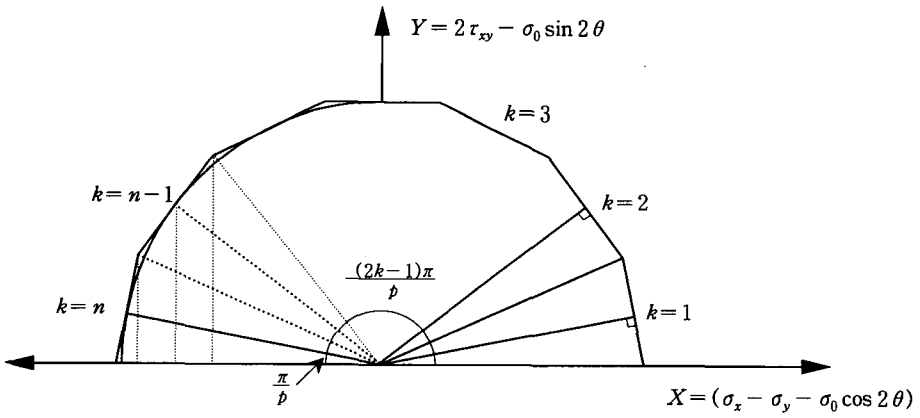

Fig. 3. External linearization of Mohr-Coulomb yield criterion using p-polygon

A_{12}^{e} = matrix constituted of A_k, B_k, C_k

$$= \begin{bmatrix} A_1 & A_2 & \cdots & \cdots & A_k & \cdots & A_{p+2} \\ B_1 & B_2 & \cdots & \cdots & B_k & \cdots & B_{p+2} \\ C_1 & C_2 & \cdots & \cdots & C_k & \cdots & C_{p+2} \end{bmatrix};$$

x_1 = matrix of nodal variable in triangular element

$= [\ u_1 \quad v_1 \quad u_2 \quad v_2 \quad u_3 \quad v_3\ ]^T$;

x_2 = matrix of element variable

$= [\ \lambda_1 \quad \lambda_2 \quad . \quad . \quad \lambda_k \quad . \quad \lambda_p\ ]^T$.

3.3.2 Plastic Flow Along Velocity Discontinuities

Four nodes along an interface of two triangles must follow the associated flow rule including vertical and tangential velocity jump along discontinuity in order to satify the kinematical admissibility.

When the Mohr-Coulomb yield criterion is applied to the discontinuity surface, the associated flow rule can be defined by Eq. (13).

Without plastic strain of continuity element itself, the local plastic strain is occuring along the velocity discontinuity surface. Fig. 4. shows a discontinuity shared by two elements.

$$\begin{aligned} \Delta u^d &= (u_b^d - u_a^d)\cos\theta^d + (v_b^d - v_a^d)\sin\theta^d \\ \Delta v^d &= (u_a^d - u_b^d)\sin\theta^d + (v_b^d - v_a^d)\cos\theta^d \end{aligned} \qquad (13)$$

where, θ^d : discontinuity surface's inclination.

The tangential velocity jump condition is set as

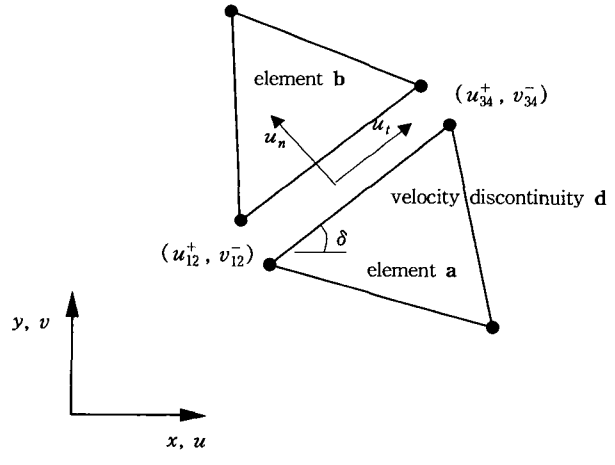

Fig. 4. Velocity discontinuity between adjacent element a and b

$(u^{d+} + u^{d-}) \geq |u^{d+} + u^{d-}|$ for computational convenience, which still gives rigorous solution of the upper analysis. This condition flexibly provides the failure formation of all triangle elements edges and also has the positive value of u^{d+} and u^{d-}. The analytical formulation of velocity jump can be expressed as in Eq. (14).

$$\begin{aligned} &(u_b^d - u_a^d)\sin\theta^d + (v_b^d - v_a^d)\cos\theta^d \\ &= |u^{d+} - u^{d-}|\tan\phi'^d \end{aligned} \qquad (14)$$

By using linear finite element, the vertical and tangential velocity jump along a discontinuity changes linearly, therefore u_a^d, u_b^d, v_a^d and v_b^d in Eq. (14) are calculated by the linear equation of velocities at node (1, 2, 3, 4) on discontinuity surface. Eq. (13) and (14) can be rewritten for a matrix formulation to be applied in numerical analysis as follows.

$$[A_{21}^d][u^d] + [A_{23}^d][w^d] = 0 \qquad (15)$$

where, $[A_{21}^d] = \begin{bmatrix} [M] & [0] \\ [0] & [M] \end{bmatrix}$,

$$[M] = \begin{bmatrix} -\cos\theta^d & -\sin\theta^d & \cos\theta^d & \sin\theta^d \\ \sin\theta^d & -\cos\theta^d & -\sin\theta^d & \cos\theta^d \end{bmatrix};$$

$$[A_{23}^d] = \begin{bmatrix} [S] & [0] \\ [0] & [S] \end{bmatrix}, \quad [S] = \begin{bmatrix} -1 & 1 \\ -\tan\phi'^d & -\tan\phi'^d \end{bmatrix};$$

$u^d = [u_1, v_1, u_2, v_2, u_3, v_3, u_4, v_4]^T$;

$w^d = [\ u_{12}^{d+} \quad u_{12}^{d-} \quad u_{34}^{d+} \quad u_{34}^{d-}\ ]^T$

3.3.3 Velocity Boundary Conditions

Fig. 5. represents the velocity boundary conditions, and the tangential velocity ($\bar{u}_1^l$, $\bar{u}_2^l$) and vertical velocity ($\bar{v}_1^l$, $\bar{v}_2^l$) at node (1,2) are shown as well.

$$\begin{aligned} \cos\theta^l u_n^l + \sin\theta^l v_n^l &= \bar{u}_n^l \\ -\sin\theta^l u_n^l + \cos\theta^l v_n^l &= \bar{v}_n^l \end{aligned} \qquad (16)$$

where, l = Number of interface; θ = interface's of inclination; n = node 1, 2 at interface.

The velocity boundary conditions can be written as a matrix formulation as Eq. (17).

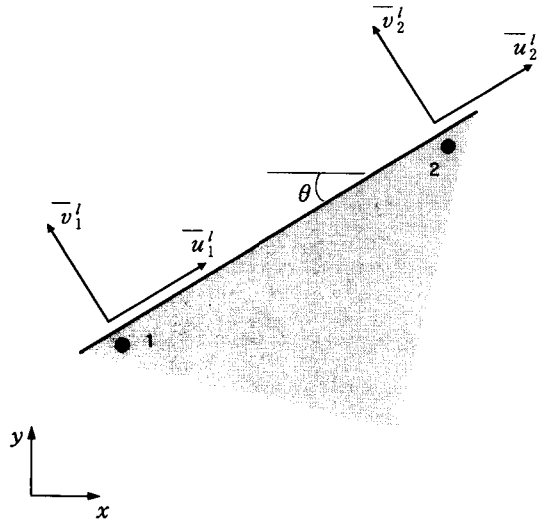

Fig. 5. Boundary edge with prescribed boundary velocity (n=1,2)

$$[A_3^l][x_1] = [B_3^l] \tag{17}$$

where, $[A_3^l] = \begin{bmatrix} \cos\theta^l & \sin\theta^l & 0 & 0 \\ -\sin\theta^l & \cos\theta^l & 0 & 0 \\ 0 & 0 & \cos\theta^l & \sin\theta^l \\ 0 & 0 & -\sin\theta^l & \cos\theta^l \end{bmatrix}$;

$x_1 = [\, u_1^l \;\; v_1^l \;\; u_2^l \;\; v_2^l \,]^T$;

$B_3^l = [\, \bar{u}_1^l \;\; \bar{v}_1^l \;\; \bar{u}_2^l \;\; \bar{v}_2^l \,]^T$.

3.4 Objective Function

The purpose of upper analysis is to find a upper bound to a rigorous collapse load satisfying kinematically admissible velocity field. The optimum value can be found by minimizing the overall energy dissipation of virtual work equation.

To define the objective function, the energy dissipation is expressed as nodal velocity, plastic and strain rate. The energy dissipation of soil element will occur along velocity discontinuity surface as well as within triangle element.

In true failure load state, the exact upper solution can be attained by the external work done by acting forces to the internal energy dissipation based on virtual work equation.

This dissipated energy due to plastic flow along the velocity discontinuities is given by integral equation as in Eq. (18).

$$\begin{aligned} P_d &= \int_L (|\tau u_t| + \sigma_n u_n)\, dL \\ &= \int_L |u_t|(|\tau| + \sigma_n \tan\phi)\, dL \end{aligned} \tag{18}$$

Eq. (18) can be rewritten by an matrix formulation to be applied in numerical analysis as in Eq. (19).

$$P_d = c_1^T x_1 \tag{19}$$

where, c_1^T = vector of constants; $x_1 = (u_1, v_1, u_2, v_2, u_3, v_3, u_4, v_4)^T$.

The energy dissipation within triangular elements represents both the associated flow rule and the yield condition at interfaces. This can be written as Eq. (20).

$$\begin{aligned} P_t &= \int_A [\sum_{k=1}^{p+2} \lambda_k (A_k \sigma_x + B_k \sigma_y + C_k \tau_{xy})]\, dA \\ &= \int [\sum_{k=1}^{p+2} \lambda_k D_k]\, dA \\ &= A \sum_{k=1}^{p+2} \lambda_k D_k \end{aligned} \tag{20}$$

where, $D_k = 2c\cos\phi + \sigma_0[\sin\phi + 1 - \frac{2\pi k}{p})]$ for $k = 1, 2, \ldots, p$; $D_k = c_i$ for $k = p+1,\ p+2$; $\lambda_k \geq 0$ for $k = 1,\ 2,\ 3, \ldots\ p+2$.

The matrix formulation of Eq. (20) for numerical analysis is as following Eq. (21).

$$P_t = c_2^T x_2 \tag{21}$$

where, c_2^T = *vector of constants*; $x_2 = [\, \lambda_1 \;\; \lambda_2 \;\; . \;\; . \;\; \lambda_{p+2} \,]^T$.

3.5 Optimization

The overall matrix formulation of optimization procedures consists of plastic strain rate, velocity boundary condition, and nodal velocity. The terms of each matrix formulation are functions of the variable of soil strength and the strength between soil mass and reinforcement.

$$\text{Minimize} \qquad C_1^T X_1 + C_2^T X_2 \tag{22}$$

where, $C_1^T X_1$ = The total power dissipation in the velocity discontinuities; $C_1^T X_2$ = The total power dissipation in the triangle

$$\text{Subject to} \quad [A_{11}][x_1] + [A_{12}][x_2] = B_1$$
$$[A_{21}][x_1] = B_2$$
$$[A_{31}][x_1] = B_3$$
$$[x_2] \geq 0.$$

4. Numerical Analyses and Results

A simple slope is assumed for the application of developed upper bound analysis program. Fig. 6. shows the geometry and boundary condition of model and it has 580 elements and 1740 nodes.

To define the material property of reinforcement, strength of reinforcement is selected as 797.12 *kN/m*, the cohesion and internal friction angle are 9.8 *kPa*, 15°, respectively. The unit weight, cohesion, and internal friction angle of the soil are 14.71 kN/m^3, 9.8 *kPa*, and 30° respectively.

Because results of upper analysis vary according to the size of finite element and the number of polygon used for approximating yield criterion, the preliminary analysis should be taken to determine both the optimum size and number of polygons. The procedure of preliminary analysis is : firstly determine the element size which will not change any limit load ; and secondly determine the number of yield polygon.

Figs. 7 and 8 show the result of preliminary analysis.

From the result of the preliminary analysis, the size of element mesh involves three element per 1 meter and 30 of yield polygons are chosen. Using this mesh size and yield polygon, upper bound analysis is carried out for the case of no reinforcement, one reinforcement, and

Table 1. Comparison of Collapse loads in limit state ($F.S = 1$)

	upper bound analysis (*kPa*)	FLAC SLOPE (*kPa*)
No reinforcement	117.48	117.28
One reinforcement	133.08	134.44
Two reinforcement	140.82	143.37

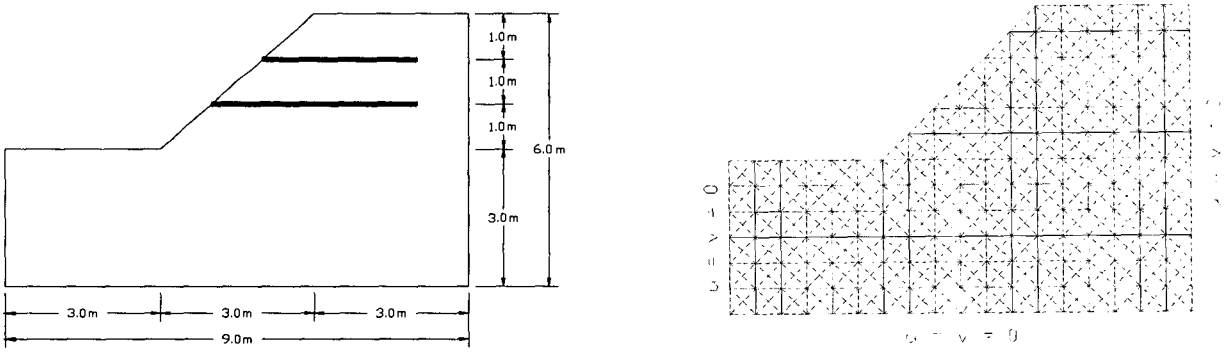

(a) Reinforced slope size (b) boundary condition

Fig. 6. Geometry of problem and finite element mesh

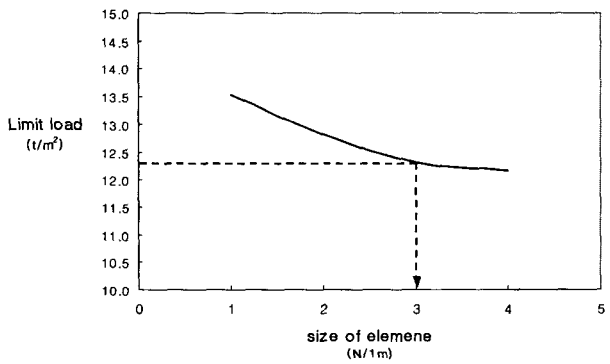

Fig. 7. Relationship between limit load and elements

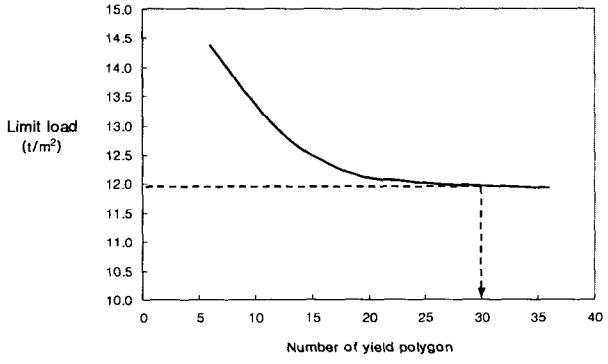

Fig. 8. Relationship between limit state and yield polygon

two reinforcement.

In addition, a well-known analysis program, FLAC is applied to the same conditions for comparative purpose. The results of the upper analysis and FLAC SLOPE, collapse, load are shown in Table 1.

Figs. 9~Fig. 11 present the plastic zones as a graphical output of upper bound analysis and FLAC SLOPE analysis. In Fig's plastic zones resulting from upper bound analysis, the darkness of element reflects the degree of internal energy dissipation, i.e., the darker, the

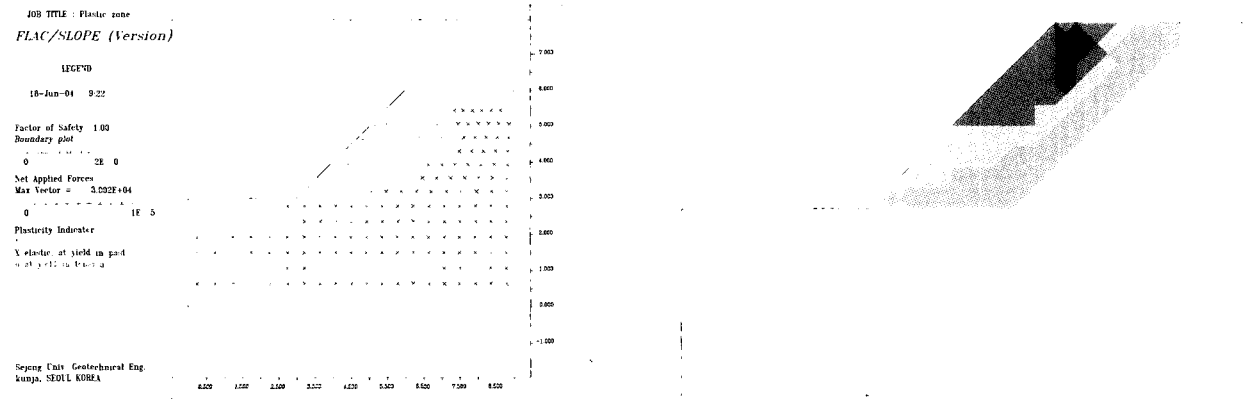

(a) Plastic zone (FLAC SLOPE) (b) Plastic zone (upper bound analysis)

Fig. 9. comparison of plastic zone for no reinforcement

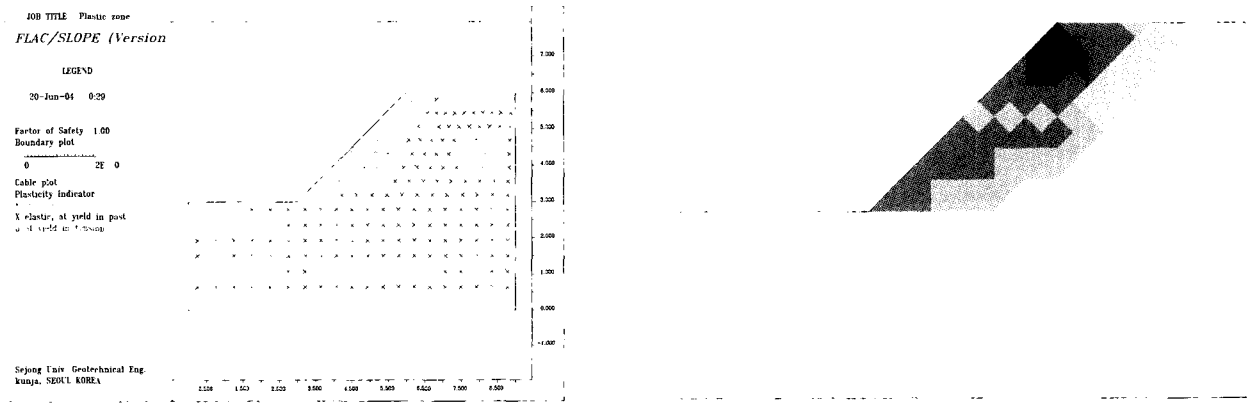

(a) Plastic zone (FLAC SLOPE) (b) Plastic zone (upper bound analysis)

Fig. 10. comparison of plastic zone for one reinforcement

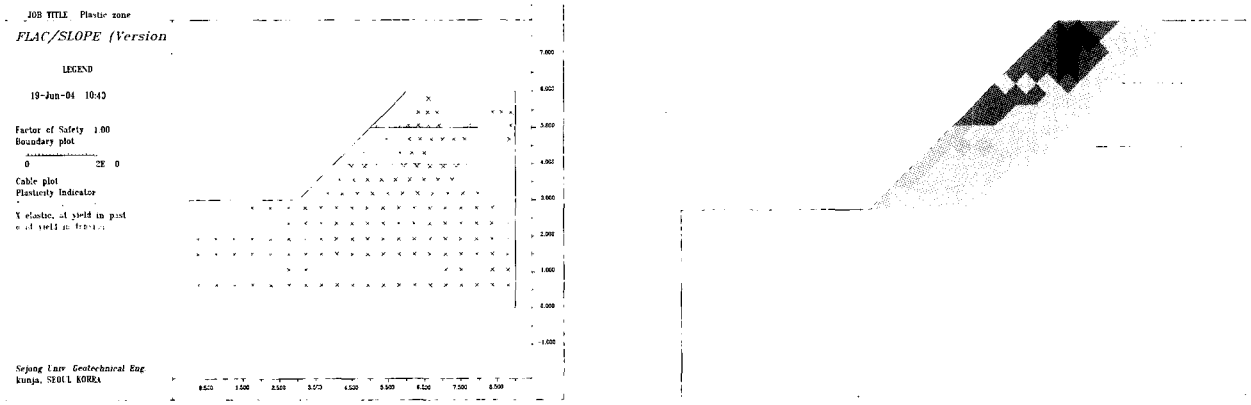

(a) Plastic zone (FLAC SLOPE) (b) Plastic zone (upper bound analysis)

Fig. 11. comparison of plastic zone for two reinforcement

more energy dissipation occurs.

It can be seem from the results of the upper bound analysis, the energy dissipation is reduced at the interfaces of concerned reinforcements. It is noticed that the bigger effect of reinforcements is on overall slope, and the smaller plastic zone is developed. In addition, for the case of no reinforcement, collapse load obtained by FLAC is smaller than that by upper bound as expected. However, for reinforced cases, collapse load obtained by FLAC is bigger than upper bound solution which is rigorous. Therefore, when reinforced slope is analized by FLAC, a special caution is required, since it may lead to unconservative design.

5. Conclusions

In this study, the limit loads acquired from the upper bound analysis considering the effect of reinforcement are compared with those of FLAC SLOPE analysis.

(1) The vertical stress and shear stress are increased by reinforcements and the upper bound analysis of interfaces movements can predict the range of failure in awareness of plasticity.

(2) The limit load is steadily increasing as much as the number of yield polygon in the upper bound analysis.

(3) This upper bound analysis is able to estimate the bearing capacity of reinforced foundation and the limit height of slope with proper techniques.

(4) There are many plastic zone at the interface between soil mass and reinforcement. This aspect implies the relationship of soil mass and the properties of reinforcements.

Referrence

1. de Buhan, P., Mangiavacchi, R., Pelligrini, G, and Selencon, J., (1989), "Yield design of reinforced earth walls by a homogenization method", *Geotechnique*, Vol.39, pp.189-201.
2. de Buhan., P. and Siad, L. (1989), "Influence of a soil-strip interface failure condition on the yield strength of reinforced earth", *Computers and Geotechnics*, Vol.7, pp.3-18.
3. J. Kim, R. Salgado, and H. S. Yu, Member, ASCE (1999), "Limit analysis of soil slope subjected to pore-water pressures", *Journal of Geotechnical and Geoenvironmental Engineering*, Vol.125, No.1, pp.49-58.
4. Sawicki, A. (1983), "Plastic limits behavior of reinforced earth", *Journal of Geotechnical Engineering*, ASCE, Vol.109, pp.1000-1005.
5. Sawicki, A. and Lesniewska, D. (1989), "Limit analysis of cohesive slopes reinforce with geotextiles", *Computers and Geotechnics*, Vol.7, pp.53-66.
6. S. W. Sloan (1989), "Upper bound limit analysis using finite elements and linear programming", *Int. J. Numer. Methods in Eng.*, Vol.13, pp.263-282.
7. S.W.Sloan and P.W.Kleeman (1995), "Upper bound limit analysis using discontinuous velocity fields", *Comput. Methods Appl. Mech. Eng.*, Vol.127, pp.293-314.

(received on Sep. 13, 2004, accepted on Sep. 24, 2004)